Supplement of Clim. Past, 21, 2083–2113, 2025 https://doi.org/10.5194/cp-21-2083-2025-supplement © Author(s) 2025. CC BY 4.0 License.





Supplement of

Hydroclimate Evolution Along Chile Over the Last 20 000 Years: insights from Leaf-Wax Hydrogen Isotope Records

Charlotte Läuchli et al.

Correspondence to: Charlotte Läuchli (laeuchli@zedat.fu-berlin.de)

The copyright of individual parts of the supplement might differ from the article licence.

Supplementary Material

This document contains:

- Sections S1 to S4
- Table S1
- Figures S1 to S14

S1. Phase II - Paleoclimate conditions

During Phase II, the onset of drier and/or warmer conditions was inferred between 17.8 ka BP and 17 ka BP at sites located south of 40°S. Specifically, this onset was estimated at ca. 17.8 ka BP from lake level lowering and the spread of North Patagonian rainforest at Lago Pichilaguna (41.3°S, Moreno et al., 2018) and the expansion of North Patagonian trees at the Huelmo site (41.5°S, Moreno and León, 2003). Note that overall humid conditions were detected at the Huelmo site until ca. 15.5 ka BP (Moreno and León, 2003). Warmer and/or drier conditions were also inferred at 17.6 ka BP at 46°S from the expansion of Nothofagus woodland reconstructed from the pollen records of the marine site MD07-3088 (Montade et al., 2013). Similar conditions were inferred after 17 ka BP from the pollen records of site ODP 1233 (41°S) and the evidence of the replacement of the North Patagonian and Subantarctic forests and parkland present during the LGM by Valdivian and Lowland Deciduous Forests characteristic of more temperate climate (Heusser et al., 2006b). The end of this overall drier phase was marked by a return to colder and/or wetter conditions detected at 14.8 ka BP from an increase in hygrophilous and cold-tolerant plants at Lago Pichilaguna (41.3°S, Moreno et al., 2018) and the expansion of the conifer Podocarus nubigena at the Huelmo site at 41.5°S (Moreno and León, 2003). On the archipelagos located off the coast of Chile, this transition was dated at 14.7 ka BP from the establishment of forests composed of Nothofagus, Pilgerodendron and Podocarpus trees characteristic of cold and wet conditions detected at the Laguna Facil and the Laguna Oprasa (44°S, Haberle and Bennett, 2004). At the Lago Lepué (42.8°S, Pesce and Moreno, 2014), this return to wetter and/or colder conditions was inferred at 14.6°S from the Eucryphia/Caldcluvia versus Podocarpaceae (P. nubigena and S. conspicua) index reflecting hydroclimate variations (ECPI, Moreno, 2004). This transition to wetter conditions was also dated at 14.5 ka BP from an increase in hygrophilous cold resistant trees at the Lago El Salto (41.6°S, Moreno and Videla, 2016) and from evidence for the development of Magellanic moorland in the pollen record at the marine site MD07-3088 (46°S, Montade et al., 2013). Several records located between 40°S and 42°S also inferred this transition at ca. 14 ka BP. These include the pollen records of Heusser et al. (2006b), Jara and Moreno (2014) and Vargas-Ramirez et al. (2008) as well as the ECPI records of Moreno (2004) and Moreno et al. (2010). Note that the record of Murali et al. (2010) suggested an onset of wetter conditions at 15.8 ka BP based on the composition of marine sediments at site ODP 1233 (41°S, Figure S13). Here, we instead refer to the records of Heusser et al. (2006a) and Kaiser et al. (2024) to reconstruct paleoclimate at 41°S since their pollen and $\delta^2 H_{wax}$ records more directly reflect past hydrological regimes.

S2. Phase III - Paleoclimate conditions

Phase III was marked by wet and cold conditions (see Sect. S1) followed by a transition period until ca. 11.5 ka BP – roughly corresponding to the Younger Dryas (ca. 12.9-11.6 ka BP). The onset of this transition period was dated at 13 ka BP from enhanced fire activity at site Lago El Salto indicting increase precipitation variability and/or seasonality (Moreno and Videla, 2016). A transition period characterized by reduced precipitation was also inferred at 12.8 ka BP from evidence for a retreat of Magellanic moorland in the pollen record at site MD07-3088 (46°S, Montade et al., 2013). A transition period starting at 12.7 ka BP was also detected from pollen and charcoal records suggesting drier conditions at the Lago Pichilaguna (41.3°S, Moreno et al., 2018) and the Lago Lepué (42.8°S, Pesce and Moreno, 2014). Jara and Moreno (2014) used pollen and charcoal records to date the onset of a decrease in precipitation at 12.4 ka BP at Lago Pichilafquén (40.7°S, pollen and charcoal records). In the record of Moreno (2004) and Moreno et al. (2010), we furthermore noted an increase in the ECPI index at around 13 ka BP indicating the onset of a transition to warmer and drier conditions. These reconstructions suggest a precipitation decrease and/or climate variability during the Younger Dryas.

Overall wet conditions were inferred until between 12.3 ka BP and 11 ka BP after which drier and warmer conditions prevailed. Specifically, the shift to warmer and drier climate was dated at 12.3 ka BP at the Laguna Facil and the Laguna Oprasa (44°S, pollen records, Haberle and Bennett, 2004) and at 12 ka BP based on the pollen records at site ODP 1233, (Heusser et al.,

2006b). The onset of a drier period was also dated at 11.6 ka BP in the pollen, charcoal and stratigraphic records of Abarzúa et al. (2004, Laguna Tahui, 42.8°S), the pollen and charcoal records at Lago El Salto (41.6°S, Moreno and Videla, 2016) and the pollen records at Lago Puyehue (40.7°S, Vargas-Ramirez et al., 2008). The pollen and charcoal records at Lago Pichilafquén (40.7°S, Jara and Moreno, 2014), at marine site MD07-3088 (46°S, Montade et al., 2013) and at Lago Condorito (ECPI index, 41.8°S, Moreno, 2004; Moreno et al., 2010) also indicated a transition to drier conditions at 11.5 ka BP. This aligns with the detection of a transition to drier and warmer conditions inferred at 11.3 ka BP at Lago Pichilaguna from the spread of drought-tolerant tree, evidence for low lake level and high frequency of fire activity (Moreno et al., 2018). Furthermore, palynological and stratigraphic changes at the Huelmo site (41.5°S, Moreno and León, 2003) as well as charcoal records and the ECPI index at Lago Lepué (42.8°S, Pesce and Moreno, 2014) confirmed a transition to drier conditions at ca. 11 ka BP. Note that this transition period was not detected in the records of Vargas-Ramirez et al. (2008), Heusser et al. (2006b), Moreno and León (2003), Haberle and Bennet (2004) and Abarzúa et al. (2004). Nevertheless, most reconstructions are consistent with a colder and wetter period between ca. 14 and 12 ka BP and the onset of drier conditions at ca. 11.5 ka BP as suggested by the $\delta^2 H_{\text{wax}}$ records at site GeoB3304-5 at 33°S.

S3 Phase IV – Paleoclimate conditions

Most records located between 40°S and 46°S indicated a transition from dry to wet conditions between 8 and 7 ka BP. At 40°S, wetter conditions were detected at 8 ka BP in the pollen records at Lago Puyehue (Vargas-Ramirez et al., 2008) and at 7.1 ka BP in the pollen and charcoal records at Lago Pichilafquén (Jara and Moreno, 2014). Note that the pollen records of Vargas-Ramirez et al. (2008) furthermore suggested an intensification of wetter conditions at 6.8 ka BP. Between 41°S and 44°S, the onset of wetter conditions was dated between 7.9 and 7.6 ka BP (Abarzúa et al., 2004; Moreno, 2004; Moreno et al., 2010, 2018; Moreno and León, 2003; Moreno and Videla, 2016; Pesce and Moreno, 2014). Specifically, wetter conditions were inferred after 7.9 ka BP from palynological and stratigraphical evidence at Laguna Tahui (42.8°S, Abarzúa et al., 2004). At the Lago Condorito (41.8°S), this transition was determined at around 7.6 ka BP based on ECPI record (Sect. S1, Moreno, 2004; Moreno et al., 2010). At Lago Pichilaguna, wetter conditions were inferred after 7.7 ka BP from stratigraphic pollen and charcoal records (Moreno et al., 2018). Furthermore, palynological and stratigraphic changes at the Huelmo site (41.5°S, Moreno and León, 2003), pollen and charcoal records at Lago El Salto (41.6°S, Moreno and Videla, 2016) as well as charcoal records and the ECPI index at Lago Lepué (42.8°S, Pesce and Moreno, 2014) confirmed a transition to drier conditions between 7.9 and 7.6 ka BP. At 44°S, Haberle and Bennett (2004) suggested seasonally wet conditions between 6.8 and 2.7 ka BP from palynological, geochemical and charcoal records. At 46°S, Montade et al. (2013) dated this transition at 7.4 ka BP using pollen records.

S4 Phase V – Paleoclimate conditions

Several records indicated climate variability along Chile during Phase V. At the Laguna Tahui (42.8°S), climate variability was suggested from changes in pollen assemblages after ca. 6.6 ka BP (Abarzúa et al., 2004). At the Laguna Facil and the Laguna Oprasa (44°S), seasonally wet climate was inferred after ca. 6.8 ka BP from palynological evidence and fire records (Haberle and Bennett, 2004). In addition, climate variability potentially related to El-Niño was inferred at these sites after ca. 2.8 ka BP (Haberle and Bennett, 2004). At the Lago Pichilafquén (40.7°S), pollen assemblage shifts and charcoal records also suggested multiple transitions from warm and dry to cold and wet conditions over the last 7.1 ka BP (Jara and Moreno, 2012, 2014). Similarly, dry intervals were detected in the pollen records at the Condorito Lake (41.8°S) between 4.1 and 3.8 ka BP and 2.9 and 1.8 ka BP despite evidence for an overall increase in precipitation between ca. 7 and 3 ka BP (Moreno, 2004). At the Lago El Salto (41.7°S), charcoal and pollen records also indicated alternating cold-wet and warm-dry phases, as well as megadrought events, after 5.3 ka BP (Moreno and Videla, 2016). At the Lago Lepué (42.8°S), dry

phases were also inferred from pollen and charcoal records between 4.3 and 4 ka BP and 2 and 0.8 ka BP despite an ECPI index suggesting a sustained shift toward wetter and colder conditions after 7.8 ka BP (Pesce and Moreno, 2014). Dry phases were also inferred at 40.8°S (Lago Puyehue and Los Mallines) from pollen records between 4.6 and 4.3 ka BP and 3 and 2.6 ka BP in the context of overall humid conditions (Vargas-Ramirez et al., 2008).

Table S1. Compiled paleoclimatic records in Chile reported in Figure 4d.

#	Ref.	Site	Lat. (WGS 84)	Long. (WGS 84)	Date range of paleoclimate reconstruct. in ka BP	Proxy type tracing paleoclimate conditions
1	Stuut and Lamy, 2004	GeoB3375-1	-27.47	-71.25	35 to 8	Humidity index (grain-size distribution)
2	Muñoz et al., 2020	core BGGC5	-30.2	-71.4	8 to 0	Pollen moisture index
3	Kaiser et al., 2008	GeoB7139-2	-30.20	-71.98	40 to 0	Terrigenous input, sedimentation rates and plant wax n-alkanes
4	Bernhardt et al., 2017	GeoB7139-2	-30.20	-71.98	26 to 0	Humidity index (grain-size distribution)
5	Ortega et al., 2012	Santa Julia archeological site	-31.83	-71.75	13 to 0	Sedimentological and geomorphological
6	Maldonado and Villagrán, 2002	Coastal swamp forest	-31.83	-71.47	6.2 to 0	Palynological
7	Maldonado and Villagrán, 2006	Swamp forest	-32.08	-71.5	10 to 0	Palynological
8	Flores-Aqueveque et al., 2021	Site GNL Quintero 1	-32.77	-71.5	28 to 21	Stratigraphic, sedimentological and geochemical
9	Jenny et al., 2002a	Laguna Aculeo	-33.83	-70.9	10 to 0	Sedimentological, mineralogical, geochemical, palynological and microfossils (diatoms)
10	Jenny et al., 2003	Laguna Aculeo	-33.83	-70.9	10 to 0	Sedimentological
11	Villa-Martínez et al., 2003	Laguna Aculeo	-33.83	-70.9	7.5 to 0	Palynological, charcoal and microalgae records
12	Valero Garcés et al., 2005	Laguna Tagua Tagua	-34.5	-71.1	46 to 6.5	Sedimentological, geochemical and palynological
13	Frugone-Álvarez et al., 2017	Lago Vichuqué	-34.8	-72.05	7 to 0	Sedimentological, geochemical
14	Heusser et al., 2006a	ODP site 202- 1234	-36.22	-73.93	140 to 0	Palynological and oxygen isotope ratios records
15	Muratli et al., 2010	ODP site 202- 1234	-36.22	-73.93	30 to 0	Petrology/Mineralogy
16	Vargas-Ramirez et al., 2008	Lago Puyehue/ Los Mallines	ca 40.7	ca72.3	17.5 to 0	Palynological
17	Jara and Moreno., 2014	Lago Pichilafquén	-40.73	-72.47	14.5 to 0	Palynological and charcoal record
18	Jara and Moreno, 2012	Lago Pichilafquén	-40.73	-72.47	2.6 to 0	Palynological and charcoal record
19	Heusser et al., 2006b	ODP site 202- 1233	-41	-74.45	50 to 9	Palynological
20	Kaiser et al., 2024	ODP site 202- 1233	-41	-74.45	50 to 0	Hydrogen isotope on leaf-wax n-alkanes
21	Moreno et al., 2018	Lago Pichilaguna	-41.25	-73.05	25 to 0	Palynological, strati. and charcoal records
22	Moreno and León, 2003	Huelmo site	-41.52	-73	20 to 7	Palynological
23	Moreno and Videla, 2016	Lago El Salto	-41.65	-73.1	16 to 0	Palynological and charcoal record
24	Moreno, 2004	Lago Condorito	-41.75	-73.12	15 to 0	Palynological, ECPI index
25	Moreno et al., 2010	Lago Condorito	-41.75	-73.12	15 to 0	Palynological, ECPI index
26	Pesce and Moreno, 2014	Lago Lepué	-42.8	-73.71	18 to 0	Palynological, ECPI index and charcoal record
27	Abarzúa et al., 2004	Laguna Tahui	-42.83	-73.5	17 to 0	Palynologic and stratigraphic
28	Haberle and Bennett, 2004	Laguna Facil/ Oprasa	ca -44.3	ca74	16.5 to 0	Palynological, geochemical and charcoal record
29	Montade et al., 2013	MD07-3088	-46.07	-75.68	22 to 0	Palynological
30	Ashworth et al., 1991	Puerto Edén	-49.13	-74.42	16 to 0	Palynological and beetle fossil record
31	Fesq-Martin et al., 2004	Gran Campo-2	-52.81	-72.93	14 to 5	Palynological
32	Lamy et al., 2010	Several sites	-51°to - 53		12.5 to 0	Palynological and sedimentological
33	Heusser et al., 2000	core HE98-1C	-53.61	-70.93	17.6 to 11.5	Palynological
34	Perren et al., 2025	Isla Hornos Lake	-55.97	-67.28	11 ka to 0	Microfossil (diatoms) record and geochemical

Figures S1 to S14

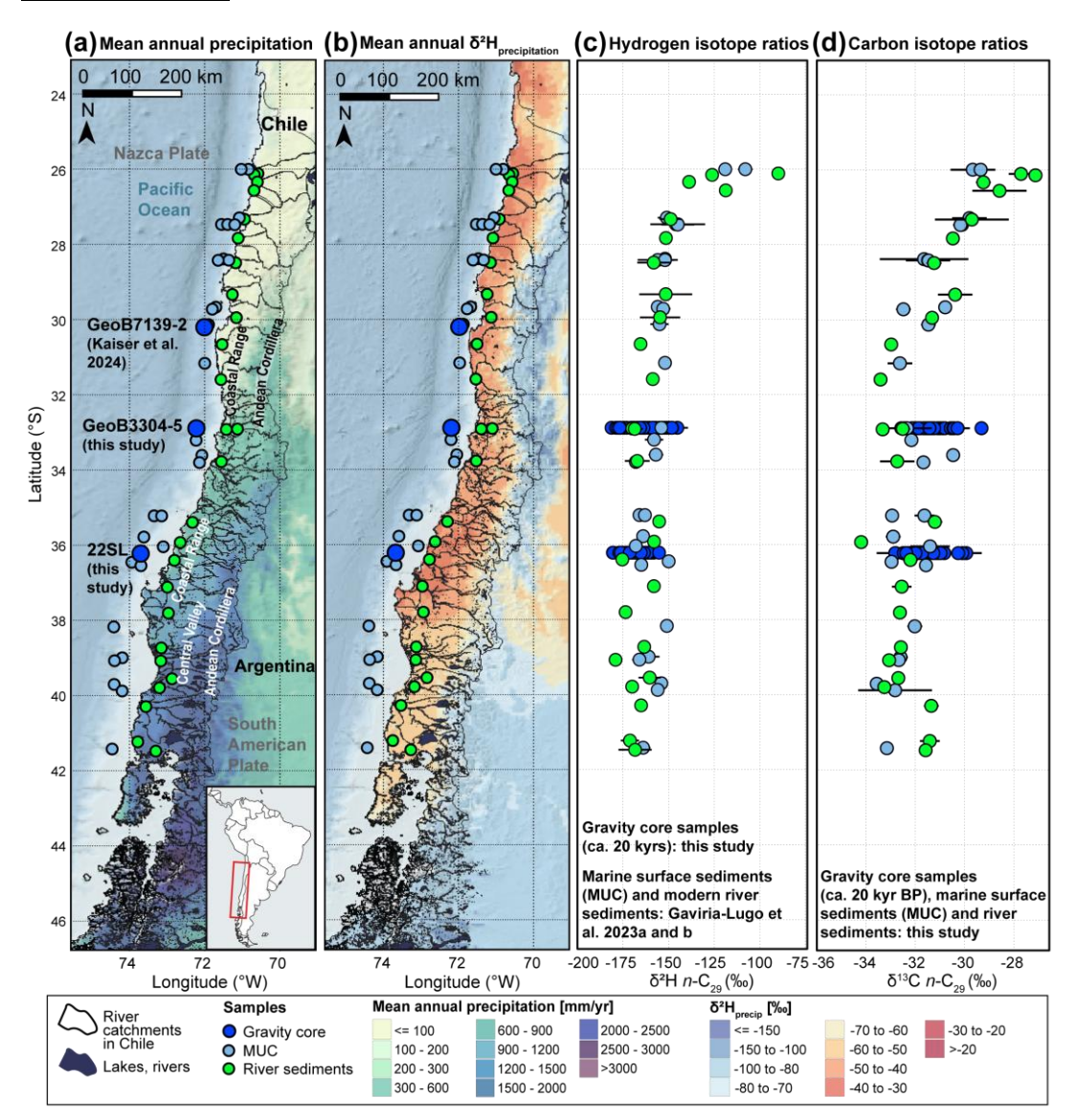


Figure S1. Sampling sites and the hydrogen and carbon isotope ratios (measured on n-C₂₉ n-alkanes) of fluvial and marine sediments along Chile. Data represent present-day conditions (river and multicorer [MUC] sediments) and variability spanning ca. 20 kyr in gravity cores. (a) Mean annual precipitation map (TRMM 3B43, European Commission, Joint Research Centre (JRC), 2015) and sampling sites (this study, Gaviria-Lugo et al., 2023a; Kaiser et al., 2024). (b) Mean annual $\delta^2 H_{precip}$ map (Bowen et al., 2005; Bowen and Revenaugh, 2003; Waterisotopes Database, 2017) and sampling sites (this study, Gaviria-Lugo et al., 2023a; Kaiser et al., 2024). (c) Hydrogen isotope composition (n-C₂₉) of modern fluvial sediments (green, Gaviria-Lugo et al., 2023a, b), marine surface sediments (MUC, light blue, Gaviria-Lugo et al., 2023a, b) and gravity cores (dark blue, site GeoB7139-2 from Kaiser et al., 2024 and sites GeoB3304-5 and 22SL) by latitude. (d) Carbon isotope composition (n-C₂₉) of fluvial sediments (green), marine surface sediments (light blue) and gravity cores (dark blue) by latitude (this study, see Gaviria-Lugo et al., 2023a for sample site description). The δ^{13} C ratio of modern river and MUC samples were corrected for the pre-industrial carbon isotope composition of the atmosphere (Section 3.4). Note the consistency of the modern hydrogen and carbon isotope ratios along Chile despite substantial changes in the mean annual precipitation amount (panel A). Digital Elevation Model is from the GEBCO Bathymetric Compilation Group (2019). The lake and river maps are from the Biblioteca del Congreso Nacional de Chile (accessed 31.03.2025). Watersheds are from Gaviria-Lugo et al. (2023a). Error bars in panels C and D correspond to two standard deviations (2σ) calculated from the $\delta 2H$ and the $\delta 13C$ values reported in Tables 5 to 7 reported in Läuchli et al. (2025, see Data availability)

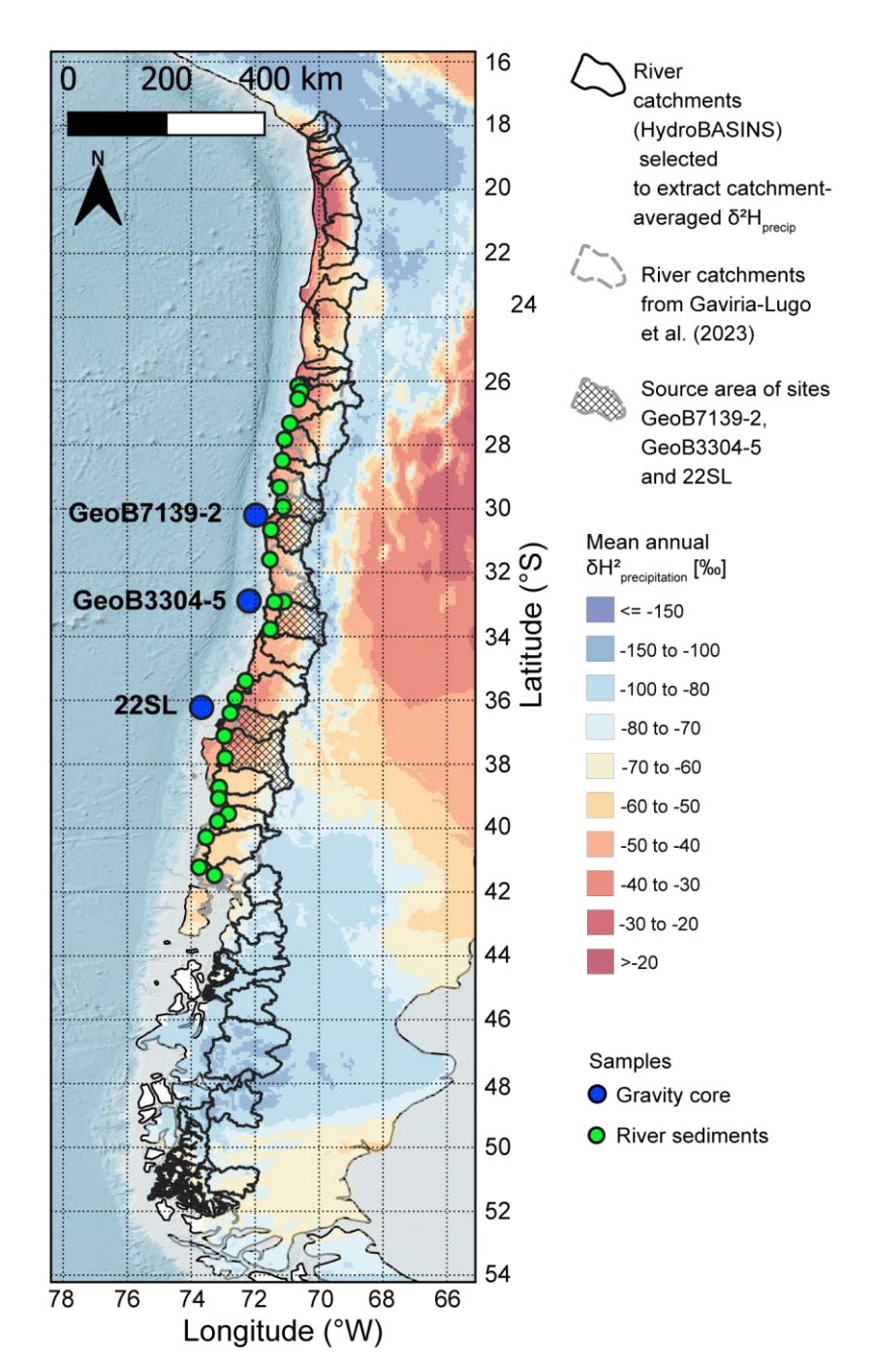


Figure S2. Catchment contours of the HydroBASINS Level 6 map (Hydroshed, Lehner et al., 2006; Lehner and Grill, 2013) compared with the catchment contours from Gaviria-Lugo et al. (2023a) with sampling sites. Fluvial sediments (green), and gravity cores (dark blue). Mean annual $\delta^2 H_{precip}$ map (Bowen et al., 2005; Bowen and Revenaugh, 2003; Waterisotopes Database, 2017). HydroBASINS map accessed the 27.03.2025. The source areas of sites GeoB7139-2, GeoB3304-5 and 22SL are indicated by the diamond line pattern. These consist, in the catchments of the Elqui, Limari, Aconcagua, Maipo, Itata and Biobío rivers listed from North to South.

Figures S3-S8: Age models

The age models of the marine sites GeoB7139-2 (Figure S3 and S6), GeoB3304-5 (Figure S4 and S7), and 22SL (Figure S5 and S8) were generated using the R-Package rbacon v. 3.2.0 (Blaauw and Christen, 2011) for the scenarios 1 and 2.

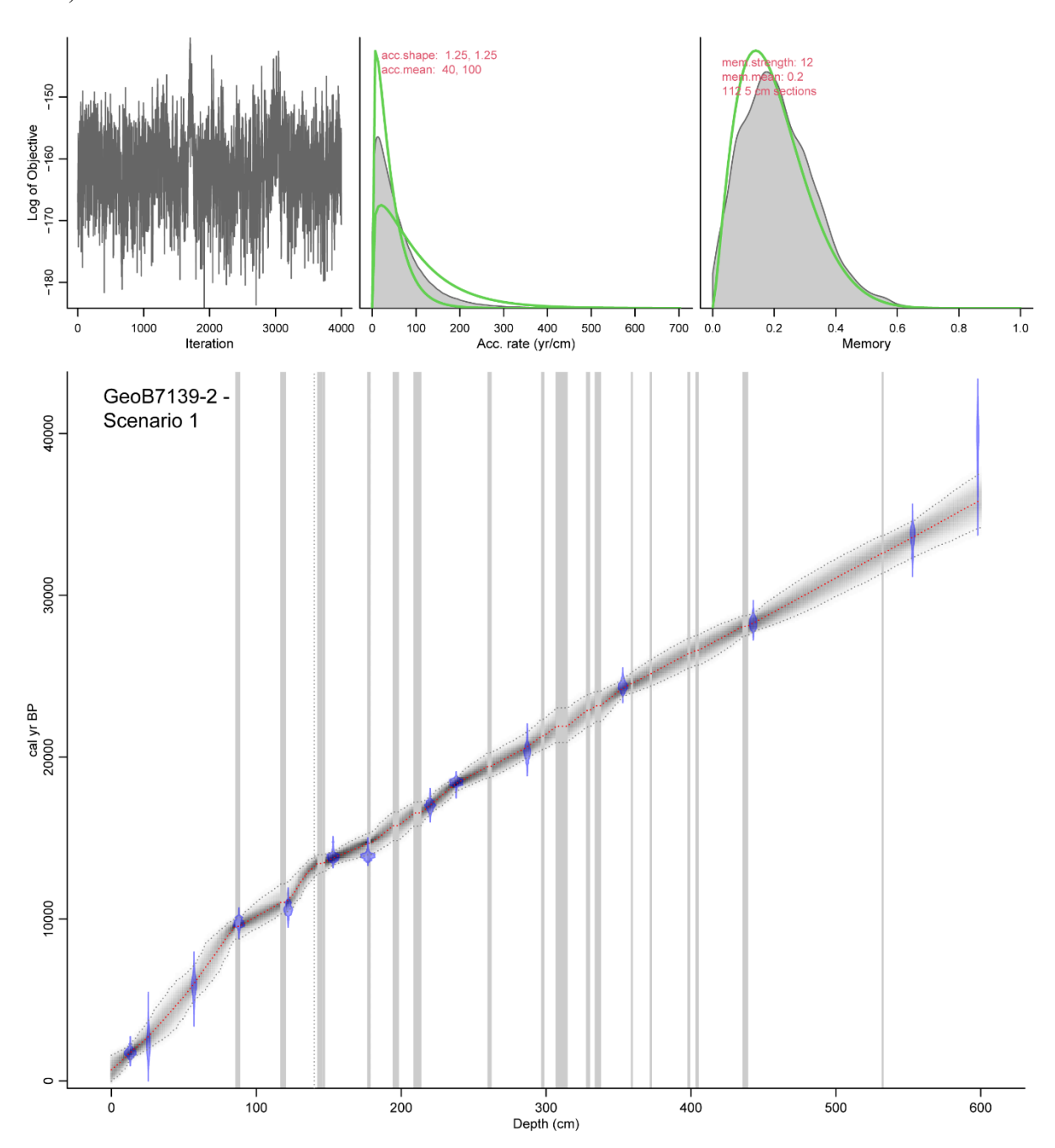


Figure S3. Age-depth model of the marine site GeoB7139-2 (Scenario 1) reconstructed and plotted using the rbacon R Package (Blaauw and Christen, 2011). A boundary was defined at 140 cm. The settings used were acc.mean=100 between 0 and 140 cm, acc.mean=40 between 140 and 600 cm, acc.shape=1.25, mem.strength=12 and mem.mean=0.2. The calibrated radiocarbon ages and their uncertainties were displayed in blue. The red and grey dashed curve corresponded to the mean and 95% confidence interval of the age-depth model, respectively. Turbidites layers were indicated by grey rectangles.

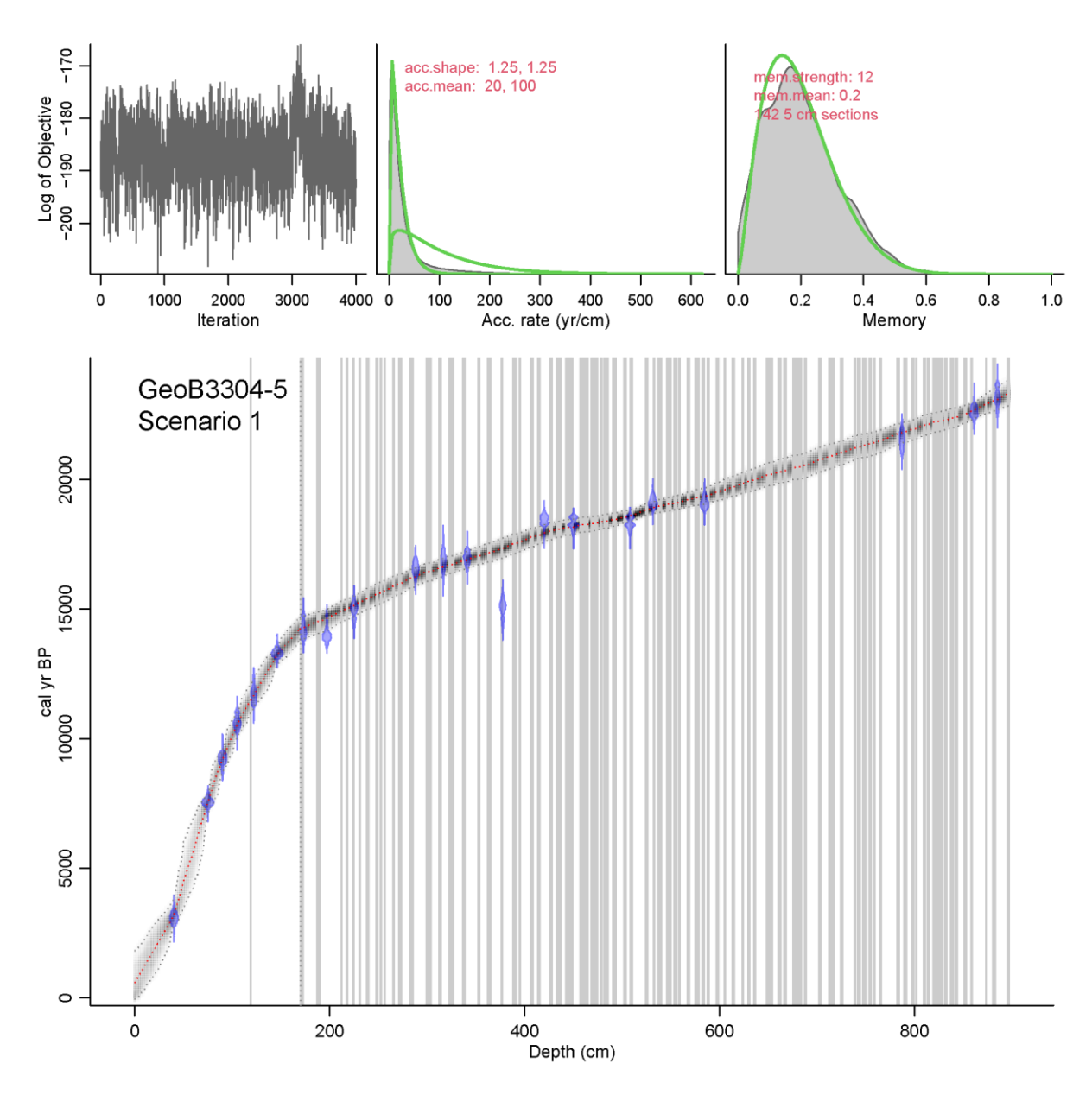


Figure S4. Age-depth model of the marine site GeoB3304-5 (Scenario 1) reconstructed and plotted using the rbacon R Package (Blaauw and Christen, 2011). A boundary was defined at 170 cm. The settings used were acc.mean=100 between 0 and 170 cm, acc.mean=20 between 170 and 897 cm, acc.shape=1.25, mem.strength=12, and mem.mean=0.2. See Figure S3 for the legend.

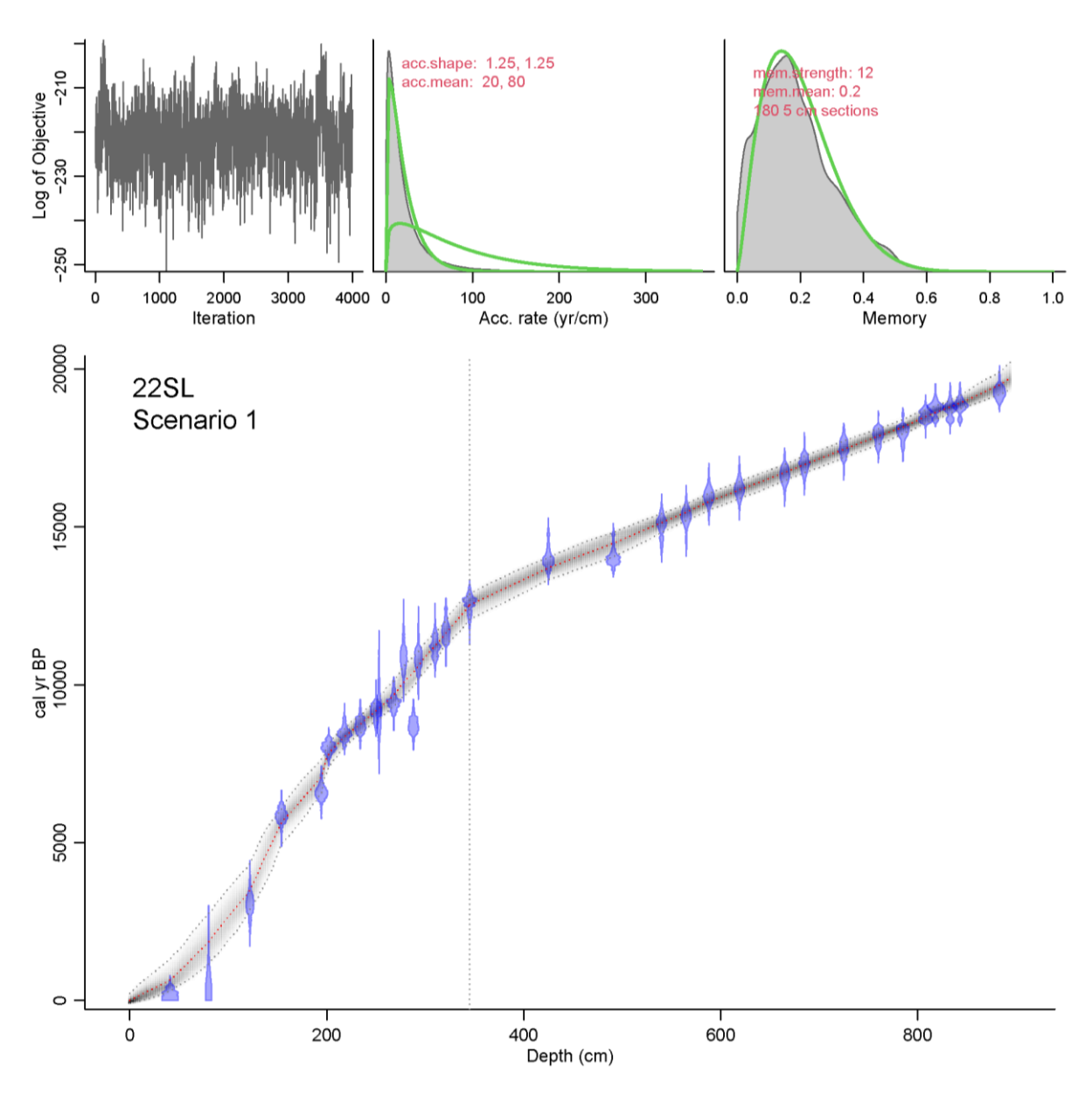


Figure S5. Age-depth model of the marine site 22SL (Scenario 1) reconstructed and plotted using the rbacon R Package (Blaauw and Christen, 2011). A boundary (dashed line) was defined at 345 cm. The settings used were acc.mean=80 between 0 and 345 cm, acc.mean=20 between 345and 894 cm, acc.shape=1.25, mem.strength=12 and mem.mean=0.2. See Figure S3 for the legend.

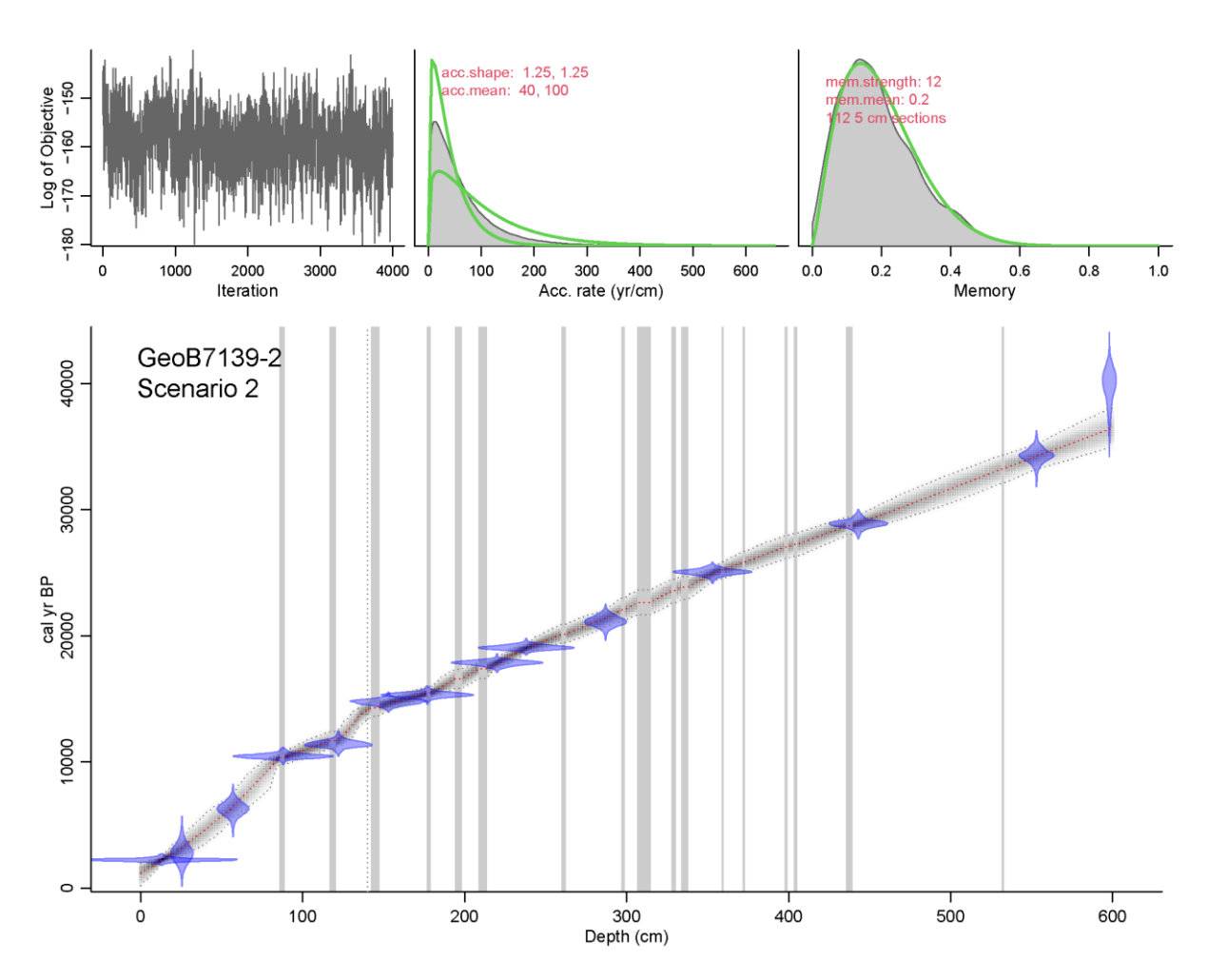


Figure S6. Age-depth model of the marine site GeoB7139-2 (Scenario 2) reconstructed and plotted using the rbacon R Package (Blaauw and Christen, 2011). A boundary was defined at 140 cm. The settings used were acc.mean=100 between 0 and 140 cm, acc.mean=40 between 140 and 600 cm, acc.shape=1.25, mem.strength=12 and mem.mean=0.2. The calibrated radiocarbon ages and their uncertainties were displayed in blue. The red and grey dashed curve corresponded to the mean and 95% confidence interval of the age-depth model, respectively. Turbidites layers were indicated by grey rectangles.

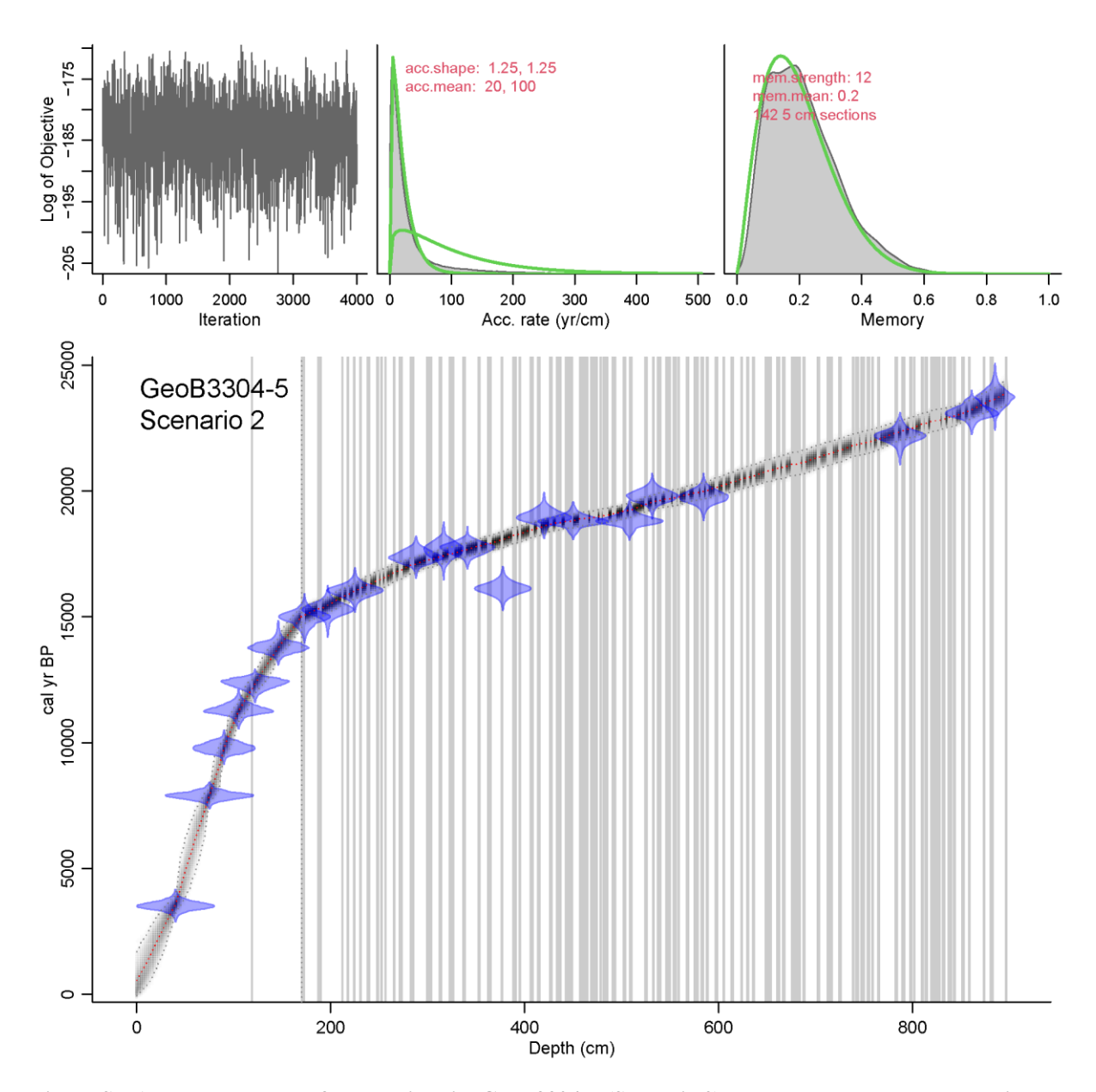


Figure S7. Age-depth model of the marine site GeoB3304-5 (Scenario 2) reconstructed and plotted using the rbacon R Package (Blaauw and Christen, 2011). A boundary was defined at 170 cm. The settings used were acc.mean=100 between 0 and 170 cm, acc.mean=20 between 170 and 897 cm, acc.shape=1.25, mem.strength=12, and mem.mean=0.2. See Figure S6 for the legend.

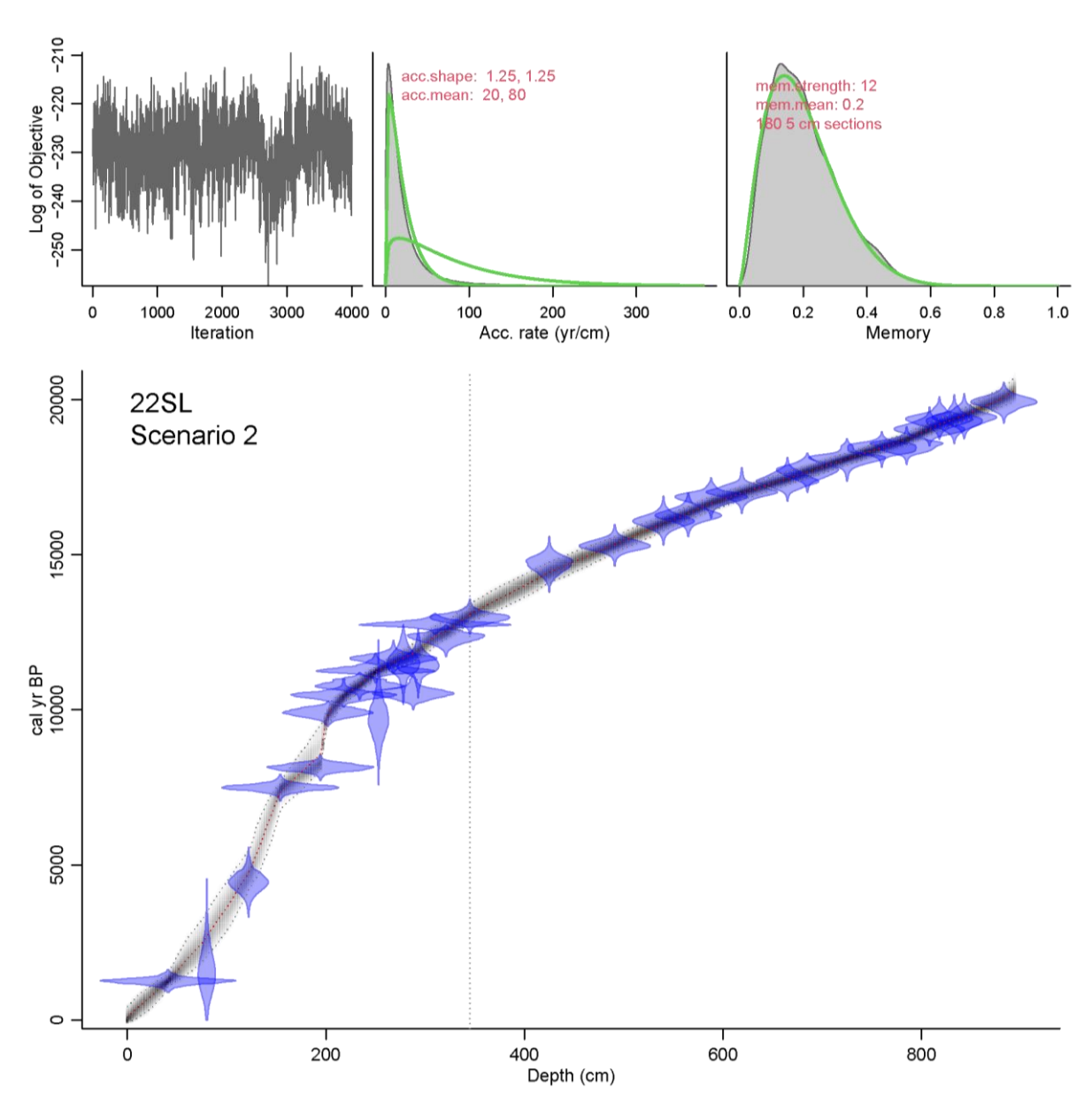


Figure S8. Age-depth model of the marine site 22SL (Scenario 2) reconstructed and plotted using the rbacon R Package (Blaauw and Christen, 2011). A boundary (dashed line) was defined at 345 cm. The settings used were acc.mean=80 between 0 and 345 cm, acc.mean=20 between 345and 894 cm, acc.shape=1.25, mem.strength=12 and mem.mean=0.2. See Figure S6 for the legend.

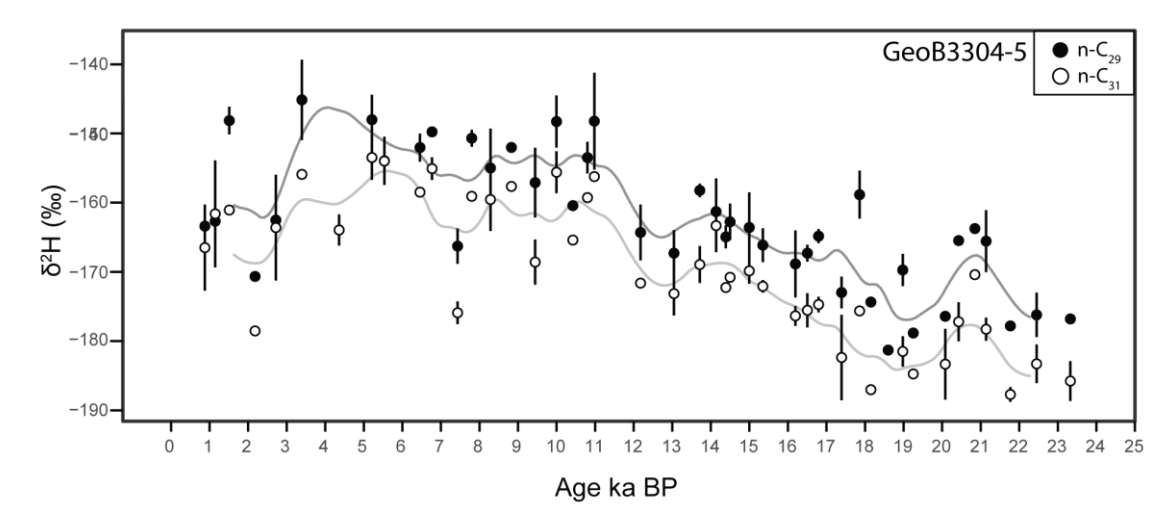


Figure S9. Hydrogen isotope records ($\delta^2 H_{wax}$) of the *n*-alkane homologues *n*-C₂₉ and *n*-C₃₁ of site GeoB3304-5. Note the similarities in the trends of the two homologues during the last 20 kyr, except at about 4 ka BP. The two standard deviations (2 σ) calculated from the values reported in the Tables S5 and S6 were indicated for the $\delta^2 H$ (*n*-C₂₉) values.

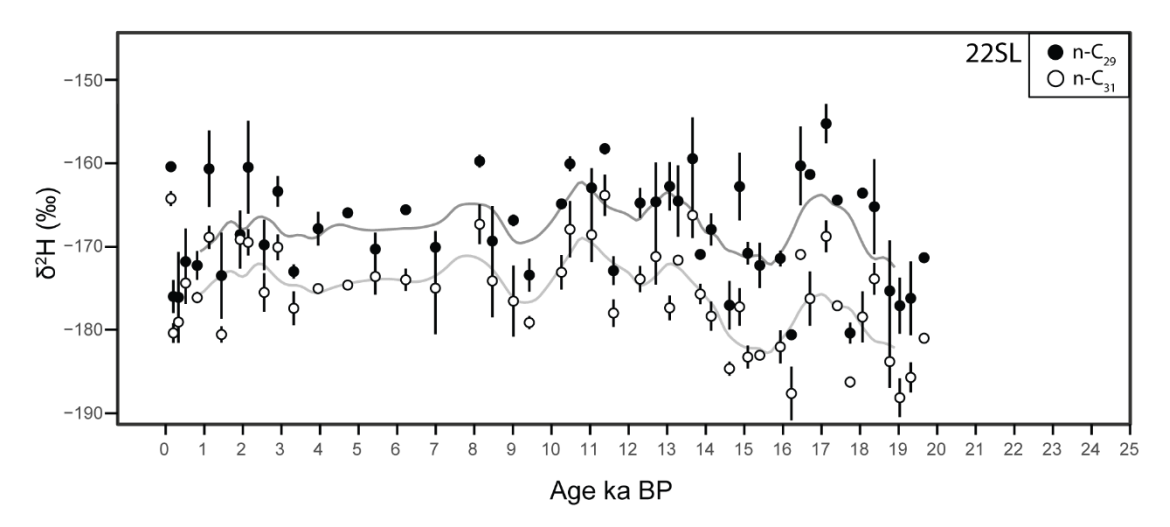


Figure S10. Hydrogen isotope records ($\delta^2 H_{wax}$) of the *n*-alkane homologues *n*-C₂₉ and *n*-C₃₁ of site 22SL. Note the similarities in the trends of the two homologues during the last 20 kyr. The two standard deviations (2σ) calculated from the values reported in the Tables S5 and S6 were indicated for the $\delta^2 H$ (*n*-C₂₉) values.

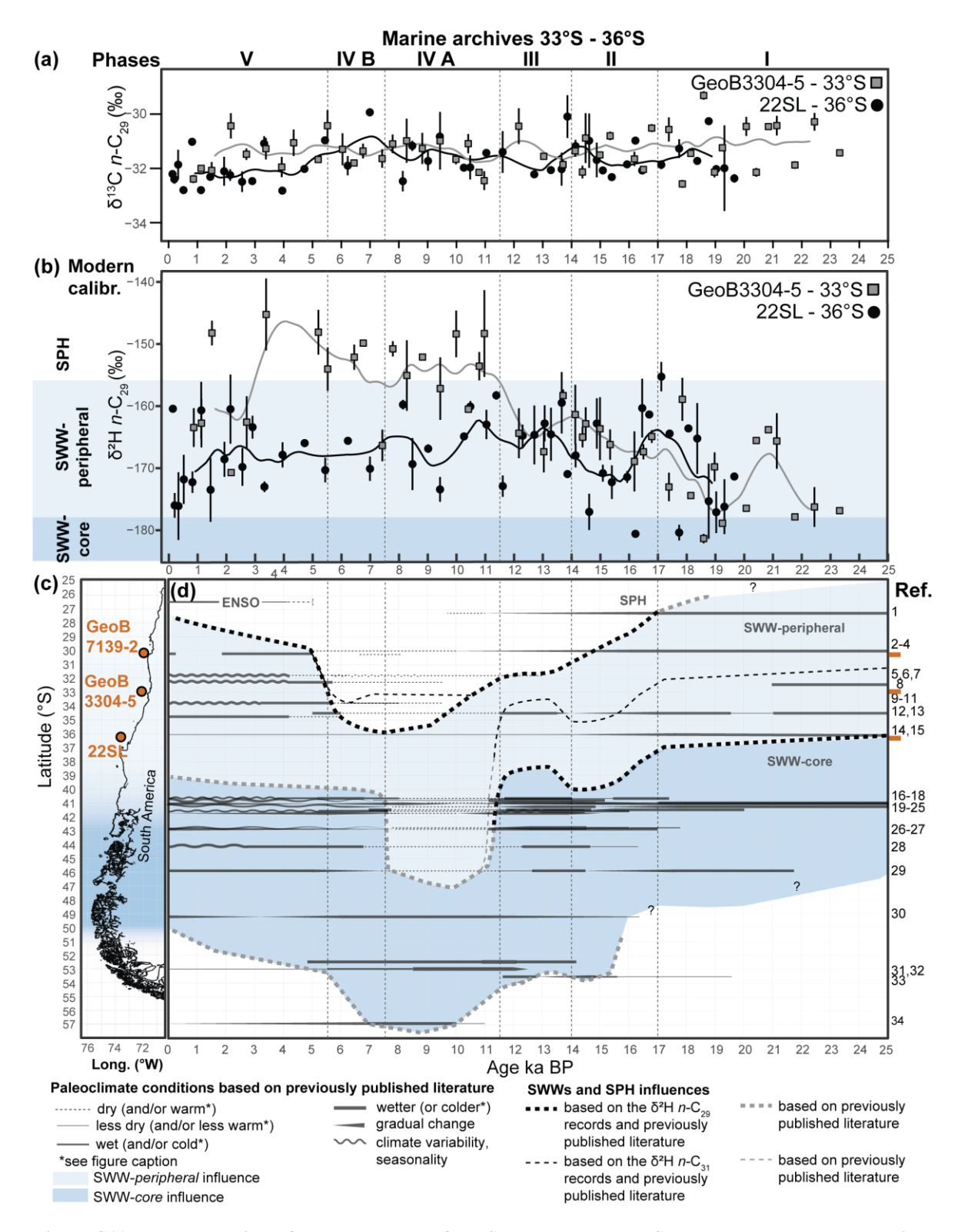


Figure S11. Reconstruction of the past extent of the SWW belt and the SPH based on the hydrogen isotope records of leaf-wax n-alkanes (n-C291) and previously published literature. (a) δ^{13} Cwax records of sites GeoB3304-5 and 22SL. (b) δ^2 Hwax records of sites GeoB7139-2 (30°S, Kaiser et al., 2024), GeoB3304-5 and 22SL. (c) Map of the west coast of South America between the latitudes of 25°S and 56°S with the locations of the marine sites. (d) Reconstruction of the past extend of the SWW belt and the SPH. Note the southward migration of the SWW belt at around 17 ka BP, its northward migration during Phase III, its abrupt shift southward during Phase IV and its return northward during Phase V. References: (1) (Stuut and Lamy, 2004), (2) (Muñoz et al., 2020), (3) (Kaiser et al., 2008), (4) (Bernhardt et al., 2017), (5) (Ortega et al., 2012), (6) (Maldonado and Villagrán, 2002), (7) (Maldonado and Villagrán, 2006), (8) (Flores-Aqueveque et al., 2021), (9) (Jenny et al., 2002), (10)

(Jenny et al., 2003), (11) (Villa-Martínez et al., 2003), (12) (Valero-Garcés et al., 2005), (13) (Frugone-Álvarez et al., 2017), (14) (Heusser et al., 2006a), (15) (Muratli et al., 2010), (16) (Vargas-Ramirez et al., 2008) in which only a cooling was recorded during the ACR, (17) (Jara and Moreno, 2014), (18) (Jara and Moreno, 2012), (19) (Heusser et al., 2006b), (20) (Kaiser et al., 2024), (21) (Moreno et al., 2018), (22) (Moreno and León, 2003), in which only a cooling was recorded during the ACR (23) (Moreno and Videla, 2016), (24) (Moreno, 2004), (25) (Moreno et al., 2010), (26) (Pesce and Moreno, 2014), (27) (Abarzúa et al., 2004), (28) (Haberle and Bennett, 2004), (29) (Montade et al., 2013) note that in this record, only cold conditions were inferred before 17.8 ka BP, (30) (Ashworth et al., 1991), (31) (Fesq-Martin et al., 2004), (32) (Lamy et al., 2010), centered at 53°S, (33) (Heusser et al., 2000), and (34) (Perren et al., 2025). See Sects. 5.3.1 to 5.3.5; Sects. S1 to S3 and Fig. S14 in the Supplementary Material for details. Error bars correspond to two standard deviations (2σ) calculated from the values reported in the Tables 5 and 6 reported in Läuchli et al. (2025, see Data availability). The gradient of blue shades in panel C schematically reflects the core and peripheral zone of the SWW belt as shown in Fig. 3.

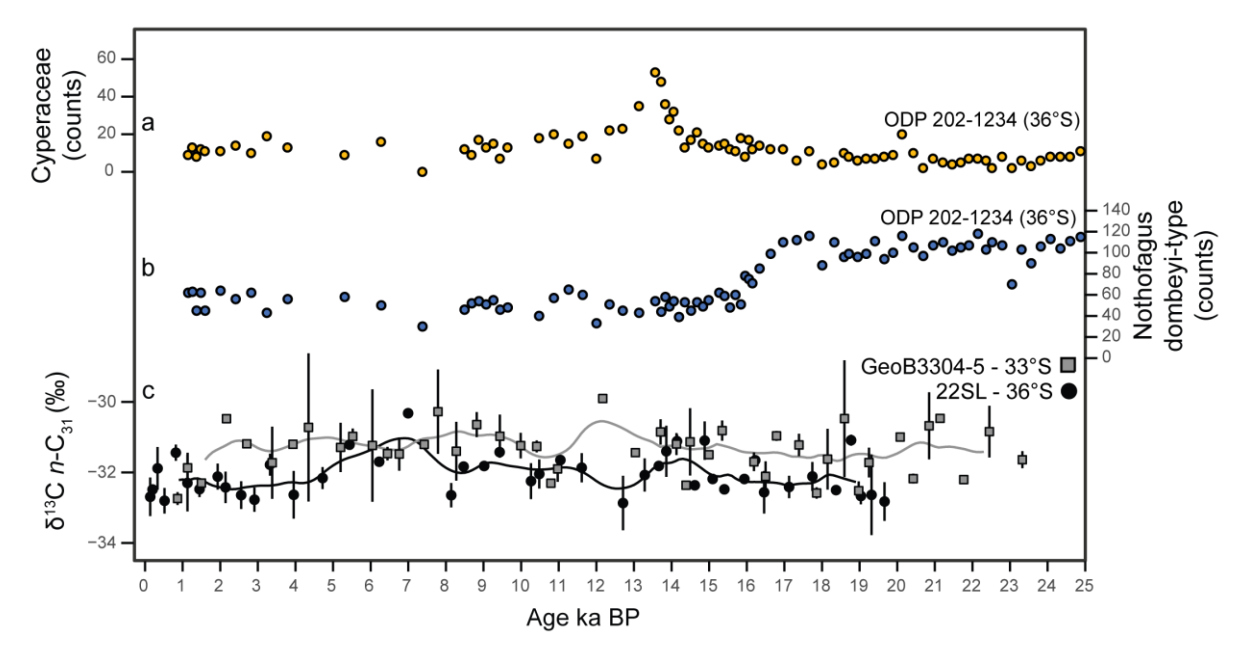


Figure S12. Comparison of the $\delta^{13}C_{wax}$ records of sites GeoB3304-5 and 22SL with pollens records of site ODP 1234 (Heusser et al., 2006a). (a) Cyperaceae counts in site ODP 1234 (36°S) from Heusser et al. (2006a) available under the ACER pollen and charcoal database (ACER project members et al., 2017; Sánchez Goñi et al., 2017) plotted using the age-depth model of Hättig et al. (2023). (b) Nothofagus dombeyi-type counts in site ODP 202-1234 (36°S) from Heusser et al. (2006a) available under the ACER pollen and charcoal database (ACER project members et al., 2017; Sánchez Goñi et al., 2017) plotted using the age-depth model of Hättig et al. (2023). (c) $\delta^{13}C_{wax}$ n-C₃₁ records of sites GeoB3304-5 and 22SL. Nothofagus dombeyi-type combines evergreen trees and Cyperaceae is a graminoid family. The lack of relationship between the $\delta^{13}C_{wax}$ record of site 22SL and these pollen records confirm that, despite changes in vegetation, the water use efficiency remains unchanged at the latitude of 33°S and 36°S in Chile over the last 20 kyr.

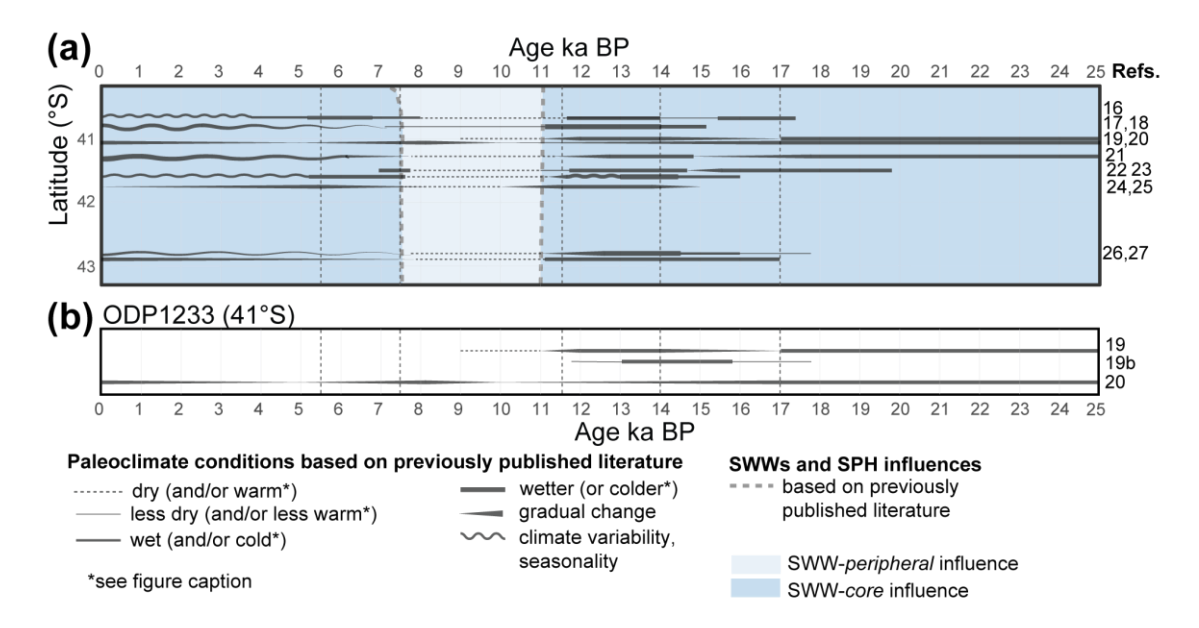


Figure S13. Reconstruction of the past extend of the SWWs based on previously published literature between ca. 40°S and 43°S. (a) Reconstruction of the past extend of the SWWs between 40°S and 43°S with relative changes in humidity and/or temperature. (b) Comparison of relative changes in humidity previously inferred at site ODP 1233 (41°S). References from Figure 4 and S11: (16) (Vargas-Ramirez et al., 2008) note that only a cooling was recorded during the ACR, (17) (Jara and Moreno, 2014), (18) (Jara and Moreno, 2012), (19) (Heusser et al., 2006b), (19b) (Muratli et al., 2010), (20) (Kaiser et al., 2024), (21) (Moreno et al., 2018), (22) (Moreno and León, 2003), note that only a cooling was recorded during the ACR (23) (Moreno and Videla, 2016), (24) (Moreno, 2004), (25) (Moreno et al., 2010), (26) (Pesce and Moreno, 2014), (27) (Abarzúa et al., 2004).

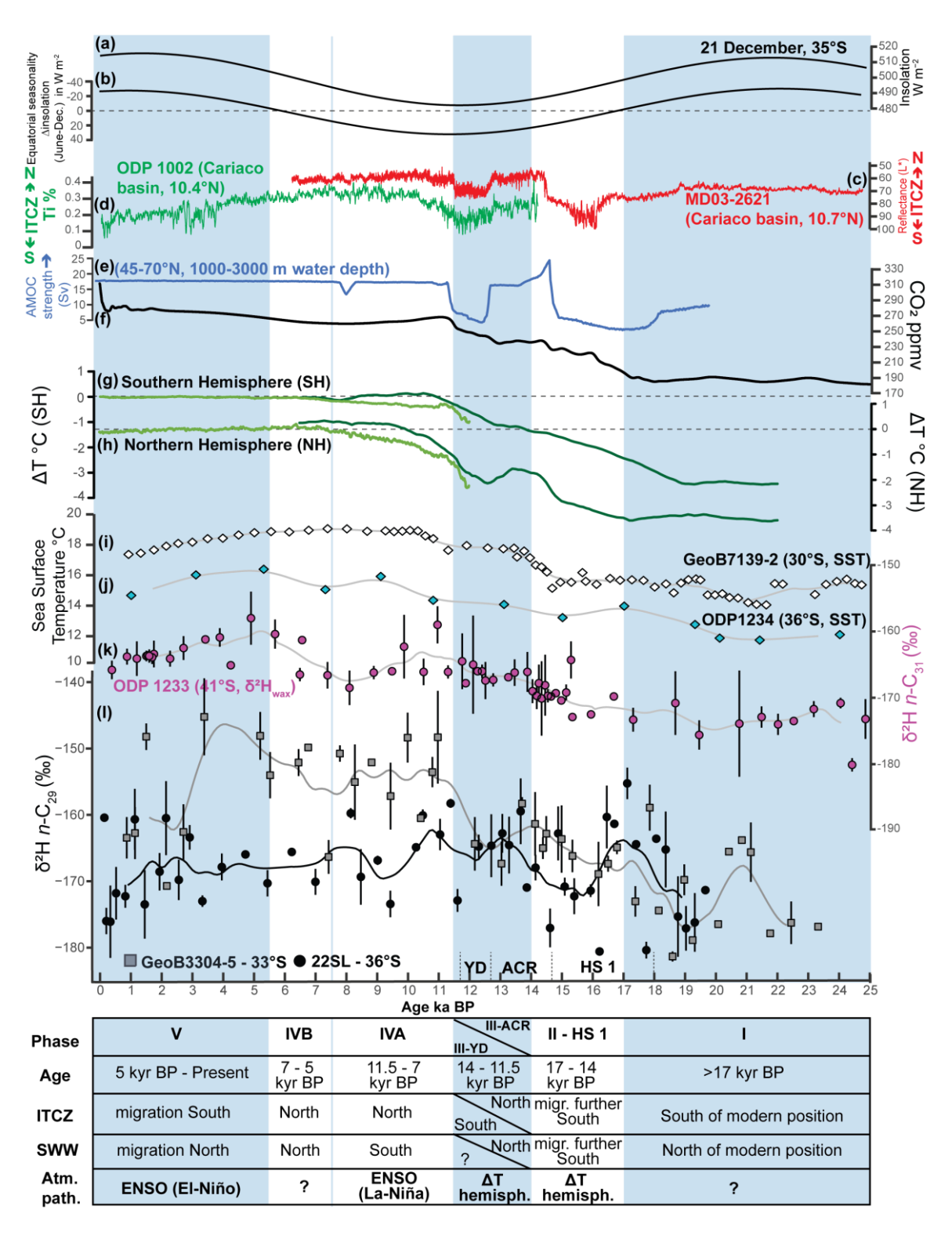


Figure S14. Comparison of the leaf-wax n-alkane hydrogen isotope records (n-C29, l) to past changes in insolation (a), seasonality (b) and independent paleoenvironmental records (c-k). (a) Equatorial seasonality modelled as the difference in insolation between June and December at the equator (Berger, 1988; Berger and Loutre, 1991). (b) Past insolation during the austral summer at the latitude of 35°S (Berger, 1988; Berger and Loutre, 1991). (c) Reflectance at site MD03-2621 indicating past latitudinal migrations of the ITCZ (Deplazes et al., 2013). (d) Titanium content of site ODP 1002 indicating past latitudinal migrations of the ITCZ (Haug et al., 2001). (e) AMOC strength derived from the model of Pöppelmeier et al. (2023) for the North Atlantic (45-70°N) between 1000 and 3000 m water depth. (f) Continuous record of atmospheric CO2 (spline-smoothed data)

compiled by Köhler et al. (2017a, b). (g) Southern Hemisphere surface temperature from Shakun et al. (2012, dark green) and Erb et al. (2022, light green) reported as temperature difference to pre-industrial values (ΔT). (h) Northern Hemisphere surface temperature from Shakun et al. (2012, dark green) and Erb et al. (2022, light green) reported as temperature difference to pre-industrial values (ΔT). (i) Sea surface temperature (Uk'37, SST) at site GeoB7139-2 (30°S, Kaiser et al., 2008, 2024). (j) Sea surface temperature (Uk'37, SST) at site ODP 1234 (36°S, de Bar et al., 2018a, b). (k) δ 2Hwax (n-C31) record of site ODP 1233 (41°S, Kaiser et al., 2024). (l) δ 2Hwax (n-C29) record of sites GeoB7139-2 (30°S, Kaiser et al., 2024), GeoB3304-5 (33°S) and 22SL (36°S). Error bars in (l) represent two standard deviations (2 σ) calculated from the values reported in Tables 5 and 6 reported in Läuchli et al. (2025, see Data availability). Abbreviations: ΔT hemisph.: atmospheric pathways driven by large interhemispheric temperature differences; ACR: Antarctic Cold Reversal; YD: Younger Dryas; HS 1: Heinrich Stadial 1.

References

Abarzúa, A. M., Villagrán, C., and Moreno, P. I.: Deglacial and postglacial climate history in east-central Isla Grande De Chiloé, Southern Chile (43°S), Quat. Res., 62, 49–59, https://doi.org/10.1016/j.yqres.2004.04.005, 2004.

ACER project members, Sanchez Goñi, M. F., Desprat, S., Daniau, A.-L., Heusser, L. E., Heusser, C. J., Mix, A. C., and McManus, J. F.: CLAM age model and pollen profile of sediment core 202-1234, https://doi.org/10.1594/PANGAEA.872844, 2017.

Ashworth, A. C., Markgraf, V., and Villagran, C.: Late Quaternary climatic history of the Chilean Channels based on fossil pollen and beetle analyses, with an analysis of the modern vegetation and pollen rain, J. Quat. Sci., 6, 279–291, https://doi.org/10.1002/jqs.3390060403, 1991.

de Bar, M. W., Stolwijk, D. J., McManus, J. F., Sinninghe Damsté, J. S., and Schouten, S.: A Late Quaternary climate record based on long-chain diol proxies from the Chilean margin, Clim. Past, 14, 1783–1803, https://doi.org/10.5194/cp-14-1783-2018, 2018a.

de Bar, M. W., Stolwijk, D., McManus, J. F., Sinninghe Damsté, J. S., and Schouten, S.: Organic geochemistry of ODP Site 202-1234, https://doi.org/10.1594/PANGAEA.892651, 2018b.

Berger, A.: Milankovitch Theory and climate, Rev. Geophys., 26, 624–657, https://doi.org/10.1029/RG026i004p00624, 1988.

Berger, A. and Loutre, M. F.: Insolation values for the climate of the last 10 million years, Quat. Sci. Rev., 10, 297–317, https://doi.org/10.1016/0277-3791(91)90033-Q, 1991.

Bernhardt, A., Schwanghart, W., Hebbeln, D., Stuut, J.-B. W., and Strecker, M. R.: Immediate propagation of deglacial environmental change to deep-marine turbidite systems along the Chile convergent margin, Earth Planet. Sci. Lett., 473, 190–204, https://doi.org/10.1016/j.epsl.2017.05.017, 2017.

Blaauw, M. and Christen, J. A.: Flexible paleoclimate age-depth models using an autoregressive gamma process, Bayesian Anal., 6, 457–474, https://doi.org/10.1214/11-BA618, 2011.

Bowen, G. J. and Revenaugh, J.: Interpolating the isotopic composition of modern meteoric precipitation, Water Resour. Res., 39, https://doi.org/10.1029/2003WR002086, 2003.

Bowen, G. J., Wassenaar, L. I., and Hobson, K. A.: Global application of stable hydrogen and oxygen isotopes to wildlife forensics, Oecologia, 143, 337–348, https://doi.org/10.1007/s00442-004-1813-y, 2005.

Deplazes, G., Lückge, A., Peterson, L. C., Timmermann, A., Hamann, Y., Hughen, K. A., Röhl, U., Laj, C., Cane, M. A., Sigman, D. M., and Haug, G. H.: Links between tropical rainfall and North Atlantic climate during the last glacial period, Nat. Geosci., 6, 213–217, https://doi.org/10.1038/ngeo1712, 2013.

Erb, M. P., McKay, N. P., Steiger, N., Dee, S., Hancock, C., Ivanovic, R. F., Gregoire, L. J., and Valdes, P.: Reconstructing Holocene temperatures in time and space using paleoclimate data assimilation, Clim. Past, 18, 2599–2629, https://doi.org/10.5194/cp-18-2599-2022, 2022.

European Commission, Joint Research Centre (JRC): South America Mean Annual Precipitation Map (TRMM 3B43 dataset), 2015.

Fesq-Martin, M., Friedmann, A., Peters, M., Behrmann, J., and Kilian, R.: Late-glacial and Holocene vegetation history of the Magellanic rain forest in southwestern Patagonia, Chile, Veg. Hist. Archaeobotany, 13, 249–255, https://doi.org/10.1007/s00334-004-0047-6, 2004.

Flores-Aqueveque, V., Ortega, C., Fernández, R., Carabias, D., Simonetti, R., Cartajena, I., Díaz, L., and González, C.: A multi-proxy reconstruction of depositional environment of a Late Pleistocene submerged site from the Central Coast of Chile (32°): Implications for drowned sites, Quat. Int., 601, 15–27, https://doi.org/10.1016/j.quaint.2021.06.005, 2021.

Frugone-Álvarez, M., Latorre, C., Giralt, S., Polanco-Martínez, J., Bernárdez, P., Oliva-Urcia, B., Maldonado, A., Carrevedo, M. L., Moreno, A., Delgado Huertas, A., Prego, R., Barreiro-Lostres, F., and Valero-Garcés, B.: A 7000-year high-resolution lake sediment record from coastal central Chile (Lago Vichuquén, 34°S): implications for past sea level and environmental variability, J. Quat. Sci., 32, 830–844, https://doi.org/10.1002/jqs.2936, 2017.

Gaviria-Lugo, N., Läuchli, C., Wittmann, H., Bernhardt, A., Frings, P., Mohtadi, M., Rach, O., and Sachse, D.: Climatic controls on leaf wax hydrogen isotope ratios in terrestrial and marine sediments along a hyperarid-to-humid gradient, Biogeosciences, 20, 4433–4453, https://doi.org/10.5194/bg-20-4433-2023, 2023a.

Gaviria-Lugo, N., Läuchli, C., Wittmann, H., Bernhard, A., Frings, P., Mohtadi, M., Rach, O., and Sachse, D.: Data of leaf wax hydrogen isotope ratios and climatic variables along an aridity gradient in Chile and globally, https://doi.org/10.5880/GFZ.3.3.2023.001, 2023b.

Group, G. B. C.: The GEBCO_2019 grid—A continuous terrain model of the global oceans and land, Liverp. UK Br. Oceanogr. Data Cent. Natl. Oceanogr. Cent. NERC, 2019.

Haberle, S. G. and Bennett, K. D.: Postglacial formation and dynamics of North Patagonian Rainforest in the Chonos Archipelago, Southern Chile, Quat. Sci. Rev., 23, 2433–2452, https://doi.org/10.1016/j.quascirev.2004.03.001, 2004.

Hättig, K., Varma, D., van der Meer, M. T. J., Reichart, G.-J., and Schouten, S.: Output age-depth data of ODP Site 202-1234, https://doi.org/10.1594/PANGAEA.957074, 2023.

Haug, G. H., Hughen, K. A., Sigman, D. M., Peterson, L. C., and Röhl, U.: Southward Migration of the Intertropical Convergence Zone Through the Holocene, Science, 293, 1304–1308, https://doi.org/10.1126/science.1059725, 2001.

Heusser, C. J., Heusser, L. E., Lowell, T. V., M., A. M., and M., S. M.: Deglacial palaeoclimate at Puerto del Hambre, subantarctic Patagonia, Chile, J. Quat. Sci., 15, 101–114, https://doi.org/10.1002/(SICI)1099-1417(200002)15:2<101::AID-JQS500>3.0.CO;2-Y, 2000.

Heusser, L. E., Heusser, C. J., Mix, A., and McManus, J.: Chilean and Southeast Pacific paleoclimate variations during the last glacial cycle: directly correlated pollen and δ 180 records from ODP Site 1234, Quat. Sci. Rev., 25, 3404–3415, https://doi.org/10.1016/j.quascirev.2006.03.011, 2006a.

Heusser, L. E., Heusser, C. J., and Pisias, N.: Vegetation and climate dynamics of southern Chile during the past 50,000 years: results of ODP Site 1233 pollen analysis, Quat. Sci. Rev., 25, 474–485, https://doi.org/10.1016/j.quascirev.2005.04.009, 2006b.

Jara, I. A. and Moreno, P. I.: Temperate rainforest response to climate change and disturbance agents in northwestern Patagonia (41°S) over the last 2600 years, Quat. Res., 77, 235–244, https://doi.org/10.1016/j.yqres.2011.11.011, 2012.

Jara, I. A. and Moreno, P. I.: Climatic and disturbance influences on the temperate rainforests of northwestern Patagonia (40 °S) since \sim 14,500 cal yr BP, Quat. Sci. Rev., 90, 217–228, https://doi.org/10.1016/j.quascirev.2014.01.024, 2014.

Jenny, B., Valero-Garcés, B. L., Villa-Martínez, R., Urrutia, R., Geyh, M., and Veit, H.: Early to Mid-Holocene Aridity in Central Chile and the Southern Westerlies: The Laguna Aculeo Record (34°S), Quat. Res., 58, 160–170, https://doi.org/10.1006/qres.2002.2370, 2002.

Jenny, B., Wilhelm, D., and Valero-Garcés, B.: The Southern Westerlies in Central Chile: Holocene precipitation estimates based on a water balance model for Laguna Aculeo (33°50′S), Clim. Dyn., 20, 269–280, https://doi.org/10.1007/s00382-002-0267-3, 2003.

Kaiser, J., Schefuß, E., Lamy, F., Mohtadi, M., and Hebbeln, D.: Glacial to Holocene changes in sea surface temperature and coastal vegetation in north central Chile: high versus low latitude forcing, Quat. Sci. Rev., 27, 2064–2075, https://doi.org/10.1016/j.quascirev.2008.08.025, 2008.

Kaiser, J., Schefuß, E., Collins, J., Garreaud, R., Stuut, J.-B. W., Ruggieri, N., De Pol-Holz, R., and Lamy, F.: Orbital modulation of subtropical versus subantarctic moisture sources in the southeast Pacific mid-latitudes, Nat. Commun., 15, 7512, https://doi.org/10.1038/s41467-024-51985-4, 2024.

Köhler, P., Nehrbass-Ahles, C., Schmitt, J., Stocker, T. F., and Fischer, H.: A 156 kyr smoothed history of the atmospheric greenhouse gases CO_2 , CH_4 , and N_2O and their radiative forcing, Earth Syst. Sci. Data, 9, 363–387, https://doi.org/10.5194/essd-9-363-2017, 2017a.

Köhler, P., Nehrbass-Ahles, C., Schmitt, J., Stocker, T. F., and Fischer, H.: Continuous record of the atmospheric greenhouse gas carbon dioxide (CO2), final spline-smoothed data of calculated radiative forcing (Version 2), https://doi.org/10.1594/PANGAEA.876013, 2017b.

Lamy, F., Kilian, R., Arz, H. W., Francois, J.-P., Kaiser, J., Prange, M., and Steinke, T.: Holocene changes in the position and intensity of the southern westerly wind belt, Nat. Geosci., 3, 695–699, https://doi.org/10.1038/ngeo959, 2010.

Läuchli, C., Gaviria-Lugo, N., Bernhardt, A., Wittmann, H., Frings, P., Mohtadi, M., Lückge, A., and Sachse, D.: Carbon and hydrogen isotope compositions of leaf wax n-alkanes, climate variables and age-depth models used to constrain hydrological regimes along Chile during the last 20,000 years., https://doi.org/10.5880/fidgeo.2025.050, 2025.

Lehner, B. and Grill, G.: Global river hydrography and network routing: baseline data and new approaches to study the world's large river systems, Hydrol. Process., 27, 2171–2186, https://doi.org/10.1002/hyp.9740, 2013.

Lehner, B., Verdin, K., and Jarvis, A.: HydroSHEDS technical documentation, World Wildl. Fund US Wash. DC, 5, 2006.

Maldonado, A. and Villagrán, C.: Paleoenvironmental Changes in the Semiarid Coast of Chile (\sim 32°S) during the Last 6200 cal Years Inferred from a Swamp–Forest Pollen Record, Quat. Res., 58, 130–138, https://doi.org/10.1006/qres.2002.2353, 2002.

Maldonado, A. and Villagrán, C.: Climate variability over the last 9900 cal yr BP from a swamp forest pollen record along the semiarid coast of Chile, Quat. Res., 66, 246–258, https://doi.org/10.1016/j.yqres.2006.04.003, 2006.

Montade, V., Combourieu Nebout, N., Kissel, C., Haberle, S. G., Siani, G., and Michel, E.: Vegetation and climate changes during the last 22,000yr from a marine core near Taitao Peninsula, southern Chile, Palaeogeogr. Palaeoclimatol. Palaeoecol., 369, 335–348, https://doi.org/10.1016/j.palaeo.2012.11.001, 2013.

Moreno, P. I.: Millennial-scale climate variability in northwest Patagonia over the last 15 000 yr, J. Quat. Sci., 19, 35–47, https://doi.org/10.1002/jqs.813, 2004.

Moreno, P. I. and León, A. L.: Abrupt vegetation changes during the last glacial to Holocene transition in mid-latitude South America, J. Quat. Sci., 18, 787–800, https://doi.org/10.1002/jqs.801, 2003.

Moreno, P. I. and Videla, J.: Centennial and millennial-scale hydroclimate changes in northwestern Patagonia since 16,000 yr BP, Quat. Sci. Rev., 149, 326–337, https://doi.org/10.1016/j.quascirev.2016.08.008, 2016.

Moreno, P. I., Francois, J. P., Moy, C. M., and Villa-Martínez, R.: Covariability of the Southern Westerlies and atmospheric CO2 during the Holocene, Geology, 38, 727–730, https://doi.org/10.1130/G30962.1, 2010.

Moreno, P. I., Videla, J., Valero-Garcés, B., Alloway, B. V., and Heusser, L. E.: A continuous record of vegetation, fire-regime and climatic changes in northwestern Patagonia spanning the last 25,000 years, Quat. Sci. Rev., 198, 15–36, https://doi.org/10.1016/j.quascirev.2018.08.013, 2018.

Muñoz, P., Rebolledo, L., Dezileau, L., Maldonado, A., Mayr, C., Cárdenas, P., Lange, C. B., Lalangui, K., Sanchez, G., Salamanca, M., Araya, K., Jara, I., Easton, G., and Ramos, M.: Reconstructing past variations in environmental conditions and paleoproductivity over the last ~ 8000 years off north-central Chile (30° S), Biogeosciences, 17, 5763–5785, https://doi.org/10.5194/bg-17-5763-2020, 2020.

Muratli, J. M., Chase, Z., McManus, J., and Mix, A.: Ice-sheet control of continental erosion in central and southern Chile (36°–41°S) over the last 30,000 years, Quat. Sci. Rev., 29, 3230–3239, https://doi.org/10.1016/j.quascirev.2010.06.037, 2010.

Ortega, C., Vargas, G., Rutllant, J. A., Jackson, D., and Méndez, C.: Major hydrological regime change along the semiarid western coast of South America during the early Holocene, Quat. Res., 78, 513–527, https://doi.org/10.1016/j.yqres.2012.08.002, 2012.

Perren, B. B., Kaiser, J., Arz, H. W., Dellwig, O., Hodgson, D. A., and Lamy, F.: Poleward displacement of the Southern Hemisphere Westerlies in response to Early Holocene warming, Commun. Earth Environ., 6, 1–10, https://doi.org/10.1038/s43247-025-02129-z, 2025.

Pesce, O. H. and Moreno, P. I.: Vegetation, fire and climate change in central-east Isla Grande de Chiloé (43°S) since the Last Glacial Maximum, northwestern Patagonia, Quat. Sci. Rev., 90, 143–157, https://doi.org/10.1016/j.quascirev.2014.02.021, 2014.

Pöppelmeier, F., Jeltsch-Thömmes, A., Lippold, J., Joos, F., and Stocker, T. F.: Multi-proxy constraints on Atlantic circulation dynamics since the last ice age, Nat. Geosci., 16, 349–356, https://doi.org/10.1038/s41561-023-01140-3, 2023.

Sánchez Goñi, M. F., Desprat, S., Daniau, A.-L., Bassinot, F. C., Polanco-Martínez, J. M., Harrison, S. P., Allen, J. R. M., Anderson, R. S., Behling, H., Bonnefille, R., Burjachs, F., Carrión, J. S., Cheddadi, R., Clark, J. S., Combourieu-Nebout, N., Mustaphi, C. J. C., Debusk, G. H., Dupont, L. M., Finch, J. M., Fletcher, W. J., Giardini, M., González, C., Gosling, W. D., Grigg, L. D., Grimm, E. C., Hayashi, R.,

Helmens, K., Heusser, L. E., Hill, T., Hope, G., Huntley, B., Igarashi, Y., Irino, T., Jacobs, B., Jiménez-Moreno, G., Kawai, S., Kershaw, A. P., Kumon, F., Lawson, I. T., Ledru, M.-P., Lézine, A.-M., Liew, P. M., Magri, D., Marchant, R., Margari, V., Mayle, F. E., McKenzie, G. M., Moss, P., Müller, S., Müller, U. C., Naughton, F., Newnham, R. M., Oba, T., Pérez-Obiol, R., Pini, R., Ravazzi, C., Roucoux, K. H., Rucina, S. M., Scott, L., Takahara, H., Tzedakis, P. C., Urrego, D. H., van Geel, B., Valencia, B. G., Vandergoes, M. J., Vincens, A., Whitlock, C. L., Willard, D. A., and Yamamoto, M.: The ACER pollen and charcoal database: a global resource to document vegetation and fire response to abrupt climate changes during the last glacial period, Earth Syst. Sci. Data, 9, 679–695, https://doi.org/10.5194/essd-9-679-2017, 2017.

Shakun, J. D., Clark, P. U., He, F., Marcott, S. A., Mix, A. C., Liu, Z., Otto-Bliesner, B., Schmittner, A., and Bard, E.: Global warming preceded by increasing carbon dioxide concentrations during the last deglaciation, Nature, 484, 49–54, https://doi.org/10.1038/nature10915, 2012.

Stuut, J.-B. W. and Lamy, F.: Climate variability at the southern boundaries of the Namib (southwestern Africa) and Atacama (northern Chile) coastal deserts during the last 120,000 yr, Quat. Res., 62, 301–309, https://doi.org/10.1016/j.yqres.2004.08.001, 2004.

Valero-Garcés, B. L., Jenny, B., Rondanelli, M., Delgado-Huertas, A., Burns, S. J., Veit, H., and Moreno, A.: Palaeohydrology of Laguna de Tagua Tagua (34° 30′ S) and moisture fluctuations in Central Chile for the last 46 000 yr, J. Quat. Sci., 20, 625–641, https://doi.org/10.1002/jqs.988, 2005.

Vargas-Ramirez, L., Roche, E., Gerrienne, P., and Hooghiemstra, H.: A pollen-based record of late glacial—Holocene climatic variability in the southern lake district, Chile, J. Paleolimnol., 39, 197–217, https://doi.org/10.1007/s10933-007-9115-0, 2008.

Villa-Martínez, R., Villagrán, C., and Jenny, B.: The last 7500 cal yr B.P. of westerly rainfall in Central Chile inferred from a high-resolution pollen record from Laguna Aculeo (34°S), Quat. Res., 60, 284–293, https://doi.org/10.1016/j.yqres.2003.07.007, 2003.

Waterisotopes Database: Global precipitation, http://waterisotopesDB.org, 2017.